Epitaxial superconducting GdBa₂Cu₃O₇-δ/Gd₂O₃ nanocomposite thin films from advanced Low-Fluorine solutions

Pablo Cayado[a], Bernat Mundet[a], Hichem Eloussifi[b], Ferrán Vallés[a], Mariona Coll[a], Susagna Ricart[a], Jaume Gázquez[a], Anna Palau[a], Pere Roura[b], Jordi Farjas[b], Teresa Puig[a] and Xavier Obradors[a,]*

[a] Institut de Ciència de Materials de Barcelona, ICMAB – CSIC, Campus UA Barcelona, E-08193 Bellaterra, Catalonia, Spain

[b] University of Girona, Montilivi Campus, Edif. PII, E17071 Girona, Catalonia, Spain

*Corresponding author: obradors@icmab.es

Abstract. We have employed the CSD method to synthesize GdBCO and GdBCO-Gd₂O₃ nanocomposite 250-300 nm thin films. For this we have designed a new Low-Fluorine (LF) solution never used before in the synthesis of GdBCO thin films that allow to reduce the HF release by 80% and increasing the reproducibility of the pyrolysis process. The growth of these thin films required the design of a new thermal process what we called "Flash-Heating" in which the heating rate is extremely fast (~600 ºC/min). The structure and the superconducting properties of the pristine GdBCO films are excellent showing a (00l) epitaxial orientation of the GdBCO grains and T_c values that reach 92.8 K which means and enhancement of more than 1 K with respect to the standard YBCO films. The calculated J_c inside the grains (J_c^G) present also remarkable values: J_c^G(5 K) ~ 40 MA/cm² and J_c^G(77 K) ~ 3.3 MA/cm². Finally, the GdBCO-Gd₂O₃ nanocomposites films, with a 20% mol of Gd₂O₃, exhibit superior superconducting properties and pinning performances with respect to the GdBCO pristine films.

Keywords. GdBCO, Low-Fluorine solution, nanocomposites, chemical solution deposition, Flash-Heating process.

1. Introduction

Nowadays, there exists a major interest in developing high temperature superconducting (HTS) materials with high performance, owing to their potential to achieve novel devices. Their properties, especially the high values of critical temperature, T_c, and critical current density, J_c, open the possibility to use them in devices working at high temperatures (in the range of liquid nitrogen) and at lower temperatures under very high magnetic fields. Among the HTS materials, REBa₂Cu₃O₇-δ (REBCO) compounds (RE=Rare Earths), which belong to the family of cuprates, have attracted the attention of scientific community due to their excellent current capabilities at high magnetic fields[1–6]. Probably, the most well-known and studied REBCO compound is YBa₂Cu₃O₇-δ (YBCO). However, in recent years it has been studied the replacement of Y³⁺ in YBa₂Cu₃O₇ by other RE ions (e.g., Nd³⁺, Sm³⁺, Eu³⁺ or Gd³⁺) to form alternative REBCO compounds because some of these compounds can display enhanced superconducting performances[7–9]. The differences in the physical properties are linked mainly to variations in structure related to modified ionic radius of the RE ions[10–13]. The modified RE size influences the distances between different planes in the structure and, therefore, the interaction between the orbitals of different atoms which leads to a change in properties of the different compounds. Additionally, the change of the RE ions modifies the thermodynamic phase diagrams and so specific changes are required in the synthesis and processing conditions of these REBCO materials. An additional difficulty is that large RE ions can display a partial substitution into the Ba²⁺ sites and hence deeply influencing the superconducting

1

properties and reducing the stability of the 123 phase in some of the *RE*BCO compounds[7,14,15].

Among the *RE*BCO compounds, the $GdBa_2Cu_3O_{7-\delta}$ (GdBCO) offers an appealing potential over YBCO [16–18]. In particular, the increase of the T_c that is observed in GdBCO bulk[7,18] and thin films[19,20], reaching up to 94-95 K, causes an upward shift of the irreversibility line which makes GdBCO a very promising material for some applications.

The first GdBCO samples studied were in form of single crystals[21] and in bulk samples[7,22]. These first samples already revealed the great properties of the GdBCO compared with other REBCO compounds. The GdBCO thin films have been prepared during many years by in-situ growth techniques, i.e. simultaneous deposition and growth. The properties of the thin films synthesized by sputtering[23–26], PLD[27] or MOCVD[28] have confirmed the results obtained in the case of the single crystals and bulk samples. However, in the search for a scalable and low-cost technique for the preparation of Coated Conductors (CCs), some researchers have focused on chemical solution deposition (CSD) as an attractive option for thin film growth[29–31]. This technique can be defined as ex-situ growth because deposition and growth are two separate steps. The case of the GdBCO films is not an exception and different works explored the CSD method to prepare GdBCO films. Most of these works were based in the well-known Trifluoroacetate (TFA) route[32] resulting in J_c of 2-4 MA/cm^2 and T_c of 93-94 K[16,19,33,34] being in good agreement with GdBCO thin films prepared by in-situ growth methods[17,20,35,36].

In order to enhance the in-field performance, we introduced secondary phases in our films forming GdBCO nanocomposites. The insertion of different secondary phases for preparing nanocomposites has been extensively investigated by many groups showing that the in-field properties of REBCO films can be vastly improved by both the "in-situ nanocomposite" and the "ex-situ nanocomposite" approaches[37–42]. In the first case complex metalorganic solutions are prepared which contain all the elements required to form the nanocomposite and the secondary phases are spontaneously segregated. In the second case, preformed nanoparticles are added to form a colloidal solution[40,41]. We have opted here for the "in-situ nanocomposite" approach, in which the NPs are spontaneously segregated in the superconducting matrix during the growth process, to include Gd_2O_3 nanoparticles (NPs) in the GdBCO films.

Despite the TFA route is an extended and well-controlled process, the fact that during the processing of the TFA-derived films HF is released to the environment has raised interest to look for alternative solutions. The so called "Low-Fluorine" solutions (LF) offers the possibility to reduce the F content and, therefore, the HF release, maintaining the same BaF_2 route for the REBCO formation than in the case of the TFA route which facilitates the processing[43]. The LF precursors have been recently investigated for the preparation of YBCO thin films, but little work has been done to grow GdBCO[33,44].

In this work we report the preparation of thin films of GdBCO using a new formulation of LF solution. The advantages of using LF over TFA (apart from the reduction of F content) are the following: the new LF solution is less sensitive to environmental humidity and also leads to films with enhanced viscoelastic properties which then results in improved homogeneities after the pyrolysis process.

The film growth process has also been investigated in relationship with the superconducting properties. It will be shown that an improved epitaxy is achieved using a new growth process called "Flash-Heating", as an alternative to the standard one used in the case of the TFA-derived films. This process minimizes the nucleation of undesired grain orientations in the GdBCO-LF films during the heating ramp and leads to high critical currents, although some granularity effects still limit the superconducting performances. GdBCO+20 mol % Gd_2O_3 films have been synthesized using the "in-situ nanocomposite" approach and we have shown that a smoothed magnetic field dependence of the critical currents, similar to YBCO nanocomposites, is achieved.

2. Solution synthesis and film preparation and characterization

2.1 GdBCO Low-Fluorine solution synthesis. The solution is prepared using three different precursor salts: gadolinium trifluoroacetate (Gd-TFA), barium acetate (Ba-OAc) and coper acetate (Cu-OAc). First, the Ba-OAc (Sigma-Aldrich ≥99,5%) is dissolved in a mixture of methanol and propionic acid (Sigma-Aldrich ≥99,5%). The amount of propionic acid added to the mixture is 26% of the final volume of the solution that is being prepared. Once the Ba-OAc is dissolved, triethanolamine (TEA, Sigma-Aldrich 98%) in an amount of 5% of the total volume of the final solution is added and homogenized during 10 minutes. After the homogenization is done, the Cu-OAc (Alfa-Aesar ≥98%) is added. After 15-20 minutes, the Cu-OAc is completely dissolved and, finally, the Gd-TFA is added to complete the solution. The solution is adjusted to the desired concentration with methanol and then placed in sealed vials under Ar atmosphere. Similar procedures were used in previous works[43–45].

In this work we have used 0.25 M GdBCO-LF solutions (with respect to Gd content of the solution) leading to films with a thickness ~250-300 nm after the conversion step, as measured by profilometer analysis. The rheological features of the 0.25 M GdBCO-LF solutions are also very similar to those recently reported for YBCO in similar solutions (Solution 4 in ref 43). This solution is also used to prepare the GdBCO-Gd_2O_3 nanocomposite. In this case, an excess of Gd-TFA is added to promote the spontaneous segregation of Gd_2O_3 .

2.2 Thin film preparation. GdBCO and GdBCO+20 mol % Gd_2O_3 films were studied in this work. The films were prepared by depositing the precursor solutions on 5 x 5 mm $LaAlO_3$ (LAO) single crystal substrates via spin coating (6000 rpm, 2 min). The subsequent standard pyrolysis and growth processes are also described elsewhere[40,46]. Flash heating process (described in detail in section 3) is also used to obtain improved texture and superconducting properties.

2.3 Thin film characterization. The microstructure and phase analysis of the grown GdBCO and 20%M Gd_2O_3 films were performed by two-dimensional (2D) X-ray diffraction (XRD) using a Bruker AXS GADDS diffractometer. This diffractometer has the same geometry of a conventional 4-circles diffractometer where on the circle is associated to a 2D detector. This allows a wide range of the reciprocal space thus allowing to analyze simultaneously the coexisting random and epitaxial crystalline phases. The radiation used is CuKα (λ_1= 1.5406 Å). The microstructure of the films at the atomic scale was analyzed with a FEI-TITAN low-base operated at 300 kV equipped with a CEOS aberration corrector. The morphology of the films after the pyrolysis and after the growth was analyzed by a Leica DM 1750 M optical microscope and a SEM Quanta 200 ESEM FEG, respectively. The granularity measurements and the superconducting properties (T_c and J_c) of the films were obtained with a Quantum design PPMS and XL-7T SQUID. Electrical contacts were prepared by evaporating silver pads and subsequently annealing under flowing oxygen, ensuring contact resistances below 10 μOhm*cm².

3. Results & discussion

3.1 Pyrolysis process: TFA vs LF solutions. The pyrolysis process used to remove the organic content of the as-deposited metalorganic solution is a critical step in CSD[47]. As demonstrated in the case of the YBCO films, the inhomogeneities that appear during the pyrolysis process due to the strong film shrinkage because of the solvent evaporation and the decomposition of the precursors degrade the final film properties[46,48,49]. To achieve smooth and defect-free films after pyrolysis is not straightforward. In the YBCO-TFA films this shrinkage can be as high as 50% of the initial thickness[46]. An additional limitation of the TFA solutions is their high hygroscopicity[50]. Even the as-deposited films are very sensitive to the humidity[16]. It

is suggested that this effect is due to the fact that the fluorine-water bonds are formed and are stronger than the fluorine-methanol bonds thus causing water absorption. This fact, together with a big difference between the values at room temperature of vapor pressure (PV) and surface tension of methanol and H_2O (PV = 3173 and 16265 Pa, and γ = 72.9 and 22.5 mN/m for H_2O and methanol, respectively), cause aggregation of the precursor species creating inhomogeneous stress in the films. This stress is likely to cause mechanical instabilities that result in film buckling or cracking, thus reducing film homogeneity after pyrolysis[46,47,51].

This problem can be partially overcome with the use of LF solutions. The LF solutions present important advantages from different standpoints: (i) the use of non-fluorinated compounds is environmentally friendly, (ii) the reduction of the TFA-salts content in the solution, the use of triethanolamine (TEA) as a ligand, which coordinates with metal ions stabilizing them and also helps to achieve a smooth release of the stress in the films during the pyrolysis due to its viscoelastic behavior. This is probably the reason why different ligands (TEA, DEA, PEG, etc.) are sometimes used to improve the quality of the CSD films and the use of propionic acid as solvent[16,43,52,53]. Finally, the use of propionic acid instead of TFA also helps to reduce the water absorption of the solution. This will lead to a higher yield of homogenous films after pyrolysis.

We have compared how the TFA and LF solutions (GdBCO-TFA and GdBCO-LF, respectively) absorb water from the ambient. The GdBCO solutions were spread over glass disks and then the mass change due to water absorption from the surrounding air was measured for each of them using a microbalance. The results are plotted in figure 1. Notice the very high water absorption of TFA films (10 wt %), that diminishes to one half for LF films. These results can be explained by the coordination of the metal ions to TEA or propionic acid that prevent their coordination with water molecules.

The reduction of the water absorption in the GdBCO-LF solutions causes an increase of film homogeneity

after the pyrolysis (more than 95% of the films without inhomogeneities) even when solutions prepared several weeks before are used. Figure 2 shows optical microscope images of the surface of two pyrolyzed films deposited on LAO substrates from solutions prepared one week before. The film made from the TFA solution presents a large amount of cracks while the film deposited from LF solution exhibits a homogeneous surface with no defects. This difference is attributed to the fact that, usually after one week, the water content in the TFA solution was well above 2 wt% (2.9 wt % in this particular case) while, in the case of the LF solution, it remained below 2 wt%.
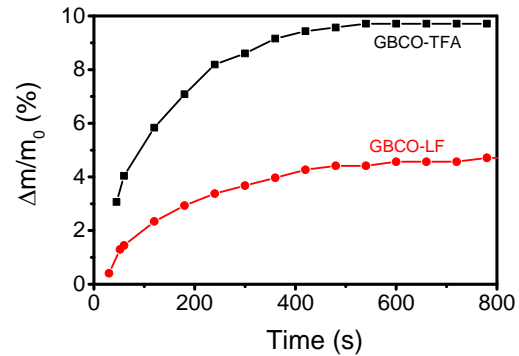

Figure 1. Mass change at room temperature in air due to water absorption of films deposited from GdBCO-TFA and GdBCO-LF solutions.
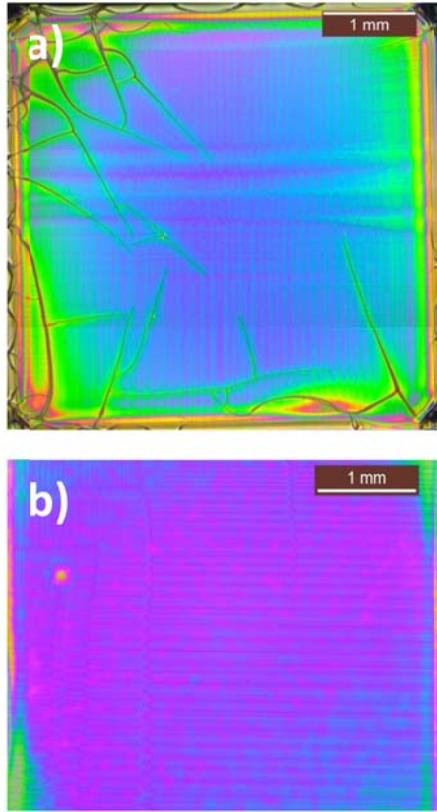
Figure 2. Optical microscope images of the surface of a pyrolyzed film deposited from 1 week old solution of: a) GdBCO-TFA and b) GdBCO-LF. The water content was much higher in the TFA solution (2.9 wt%) what explains the appearance of cracks that are absent in the LF film.

The above features of the GdBCO-LF solution allow us to obtain reproducible films. So, from now on, we will focus in this LF solution. However, its use requires to modify the standard thermal process for the pyrolysis of the TFA- solutions. We have used a thermal process already reported for YBCO-LF[43]. It is similar to the one used for the TFA solutions but with a higher dwell temperature (500 ºC) and a higher gas flow rate (0.12 l/min) to favor the complete decomposition of the TEA.

3.2 Growth process: Flash-Heating process. The phase diagram of the GdBCO reported by Iguchi *et al.* and Lee *et al.* shows that the stability[35,54] and peritectic[55] lines are shifted towards higher temperatures, as compared to YBCO. This suggests that the crystallization of GdBCO films should be optimum at higher temperatures than in the YBCO films. It is also noticeable that in most of the works devoted to the GdBCO films synthesis lower values of P_{O_2} are used[16,33,35]. So we concentrated in exploring growth conditions shifted to higher crystallization temperatures and lower oxygen partial pressures (P_{O_2}), as compared to standard growth process for the YBCO-TFA films[31,56,57]. However, increasing the crystallization temperature to 820 ºC (dwell time: 180 min) and reducing P_{O_2} to 1.10^{-4} atm (100 ppm) did not lead to fully satisfactory results. While the obtained T_c values were improved when P_{O_2} was reduced, the 2D XRD pattern shown in figure 3a) demonstrates that the film is not completely epitaxial, some fraction of polycrystalline grains still remains and the film texture of the c-axis oriented grains is not of high quality. The ring that appears with the spots in the (00l) Bragg´s positions indicates that the c-axis oriented grains tend to grow with a certain degree of misorientation. Also, the presence of a ring corresponding to the (103)GdBCO Bragg peak confirms that randomly oriented grains have been also formed. Finally, we also notice the spot associated with (200)GdBCO Bragg´s peak which means that there are also some grains that nucleate epitaxially with the a-b plane perpendicular to the substrate. The Bragg´s peaks associated to (102) reflection, identified with an arrow in figure 3a) can be better identified in the integrated pattern shown in figure 3 b).

5
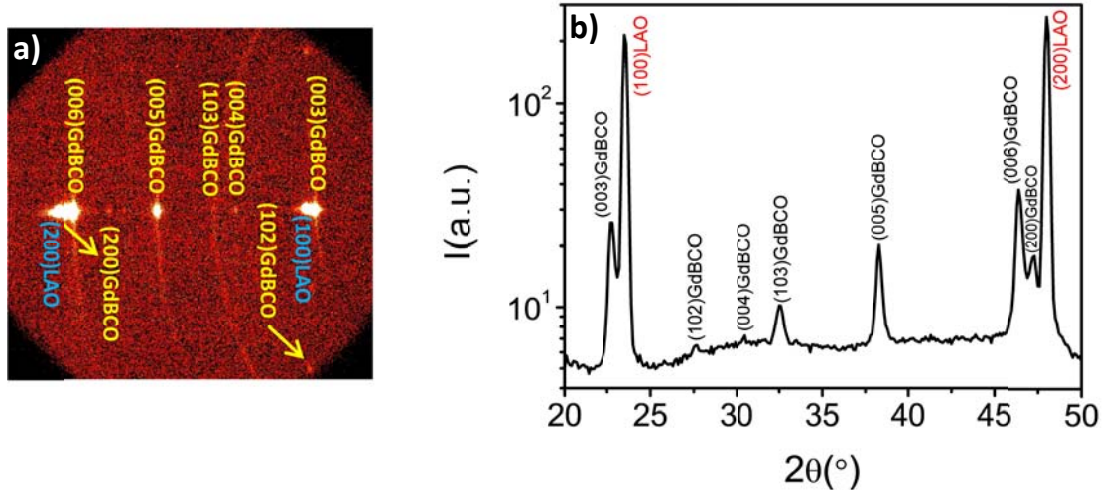
Figure 3. 2D XRD θ-2θ frame a) and integrated pattern b) of a GdBCO-LF film grown using the modified standard process (crystallization temperature= 820 ºC and P_{O_2}=100 ppm).

The existence of undesired nucleation under these conditions is also clearly evidenced in the SEM image shown in Figure 4. In this image we can see that the nucleation of a-axis is promoted. This is something not observed in in the case of YBCO-LF films which show a perfectly c-axis oriented films using similar processing conditions[43].
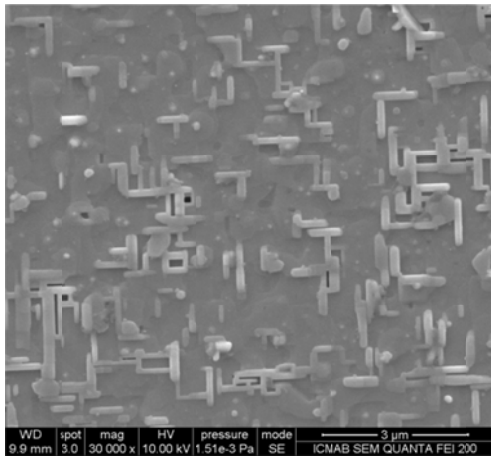
Figure 4. SEM image of a GdBCO-LF film prepared following the standard process used for the growth of YBCO-TFA films. At the used processing conditions the a-axis nucleation is clearly enhanced.

In order to investigate the reason why the films do not crystallize only with the c-axis epitaxial orientation, a film quenching study at different temperatures was performed. The results shown in figure 5 provide the clues to discern the origin of the problem. Under the presently used nucleation and growth conditions[25-27], the GdBCO phase nucleates at temperatures in the range of 710-725 ºC but at these temperatures the heterogeneous nucleation of GdBCO leads to multiple nuclei orientations oriented perpendicular to the substrate interface (c-axis, a-b plane and may be even <103> axes) because we are in the region of high supersaturation conditions[31,58]. We observe that the (103) peak is the first observed when temperature is increased (between 710 and 725 ºC), thus suggesting that homogeneous nucleation, leading to randomly oriented grains, occurs before the c-axis oriented epitaxial grains ((00l) peaks appear between 750 and 790 ºC). It cannot be discarded, however, that some heteroepitaxial nucleation of grain with <103> axes perpendicular to the substrate first appear and later leading to randomly oriented grains which contribute to the observed (103)GdBCO Bragg peak. In any case, this suggests that under these particular conditions the GdBCO crystalline phase forms under an excessive supersaturation where the nucleation barriers for the different crystalline orientations are too close to that of the c-axis oriented nucleation.
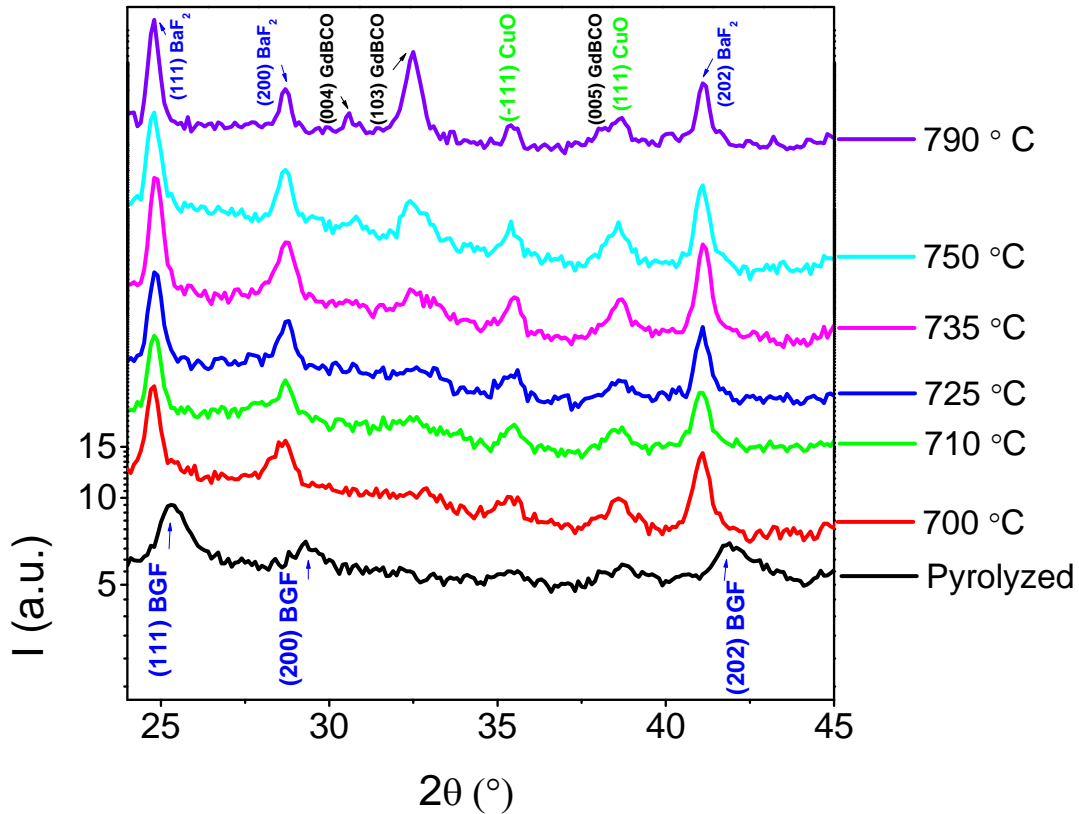
6

Figure 5. 2D XRD θ-2θ integrated patterns of GdBCO-LF films quenched after annealing at different temperatures showing that nucleation of randomly oriented grains (presence of (103) Bragg´s reflection) occurs before that the epitaxial grains ((00l) Bragg´s reflections).

It is well known that c-axis oriented grain nucleation is more favorable at high temperatures for *RE*BCO structures[31,58]. This is because at high temperatures, where supersaturation is lower, the difference in the nucleation barriers, and so the nucleation rates, between the a-b axis oriented grains, the randomly oriented grains and the c-axis oriented grains is larger, even if all the nucleation rates are lower[59]. Therefore, it is interesting to accelerate, as much as possible, the transition through intermediate temperatures where non-desirable nucleation events may occur. This will not allow enough time to induce multiple nucleation events at low temperatures and so reaching the crystallization temperature as fast as possible to favor the nucleation of c-axis grains. With this aim, a "Flash-Heating" process was designed. This process is similar to the one reported by Erbe *et al.*[16]. The furnace is first pre-heated at the dwell temperature (820 ºC in this case) and then the film is introduced directly at this temperature. With this procedure it is possible to reach average heating ramps of ~600 ºC/min, more than 20 times faster than the 25 ºC/min of the original process. The XRD patterns of the films grown using this type of process are presented in figure 6. A perfectly epitaxial (00l) GdBCO films with no presence of other orientations or other phases are achieved with our "Flash-Heating" process.
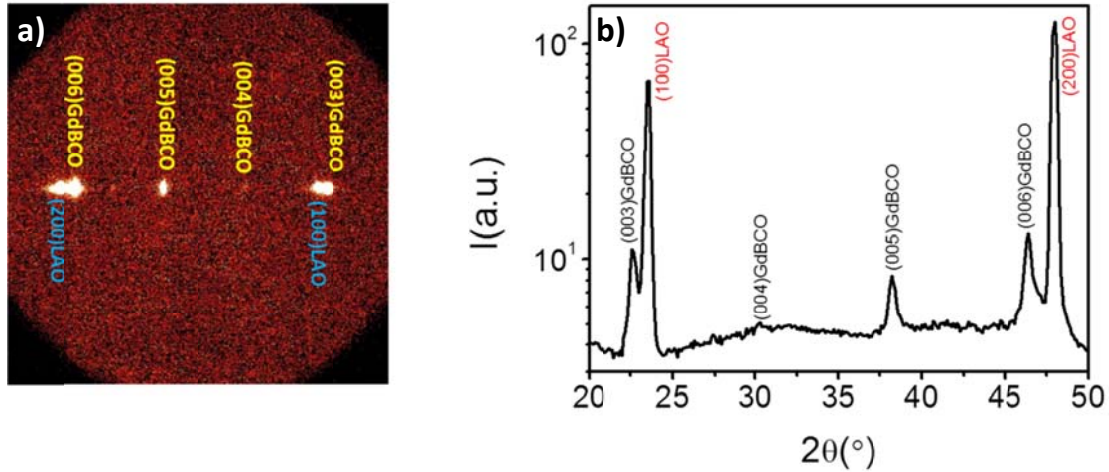
Figure 6. a) 2D XRD θ-2θ frame and b) integrated pattern of GdBCO-LF films grown using the Flash-Heating process at 820 °C.

Despite that the XRD patterns do not show the presence of other crystal orientations, in the SEM images (figure 7) it is still possible to observe a small amount of a-b grains (white arrows) and some pores (black spots). This means that the thermal process is still not fully optimized and there is still some room for improving the processing conditions. Healing the porosity in CSD films is a complex issue strongly dependent on film thickness which may be tuned through annealing temperature and time, however, it is also necessary to avoid film dewetting which may be promoted at excessive heating temperatures[60].
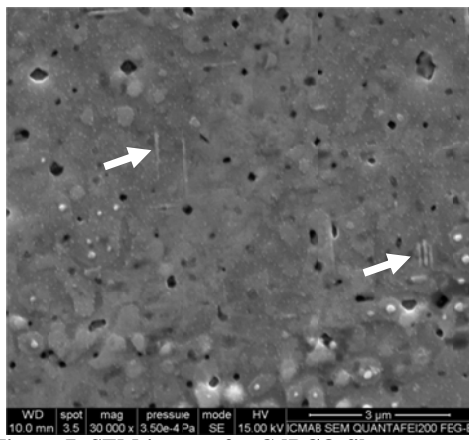

Figure 7. SEM image of a GdBCO film prepared by Flash-Heating process showing a small amount of a-b grains (indicated with white arrows) and some pores (black spots).

Nonetheless, at this stage, the films present $T_{c, onset}$ of 92.6 K with a ΔT_c=10.1 K

(see Figure 8 (a)) which is similar to the best results previously reported for GdBCO-TFA and GdBCO-LF films[16,20,35,44]. However, moderate values of self-field critical current densities, J_c^{sf} at 5 K ~12.5 MA/cm^2 and J_c^{sf} at 77 K ~1.5 MA/cm^2, were registered (see Figure 8 (b)).
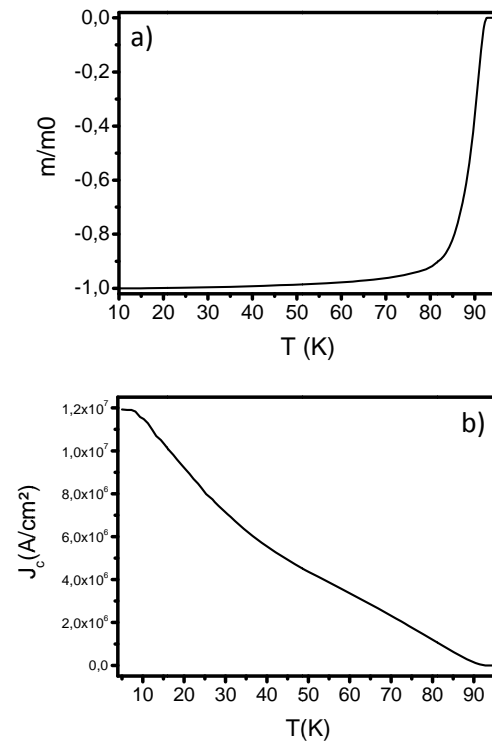

Figure 8. Inductive measurements on a GdBCO-LF film grown by using the flash-heating process showing a) the low field magnetizations vs temperature allowing to determine the T_c and b) the measured temperature dependence of the self-field $J_c(T)$.

The values of J_c reported in figure 8 are very likely affected by the presence of a small amount of a-b grains which behave as barriers for percolative current. The presence of these a-b grains and also the porosity that is observed in figure 7 produce inhomogeneities in the film that could induce a granular behavior for the current flow[61–64]. Granularity in superconductors is characterized by the existence of two different critical current densities: one inside the grains (J_c^G) and another one associated with the grain boundary network (J_c^{GB}). It is possible to determine the J_c^G by applying the method reported by Palau et al[64]. We investigated, therefore, if granularity could be at the origin of the reduced J_c^{sf} values in our films. It has been widely investigated by several authors how percolative current blocking can be observed in thin films and how this influences J_c^{sf} values. The existence of granularity can be experimentally identified by performing hysteresis loops at different maximum applied fields[63,64]. Figure 9 displays a set of such hysteresis loop measurements with a maximum magnetic field of 8 T measured at 5 K. It is observed that the maximum value of the magnetization at the reverse branch appears approximately at an applied field of 0.4 T. For a single crystalline superconducting film this would be expected at zero field. The displacement of the maximum value of the magnetization to higher fields is attributed to granularity effects. The magnetization peak appears when the return internal magnetic field at the grain boundaries is compensated by the applied field[65]. The obtained grain size is 0.5 μm and the J_c^G values for the GdBCO film measured in figure 9 by applying this method are: J_c^G(5 K)~40 MA/cm^2 and J_c^G(77 K)~3.3 MA/cm^2 (determined with the same kind of measurements at 77 K). These results show that, if the granularity could be avoided by optimizing the processing conditions, the performances of the GdBCO-LF films might be largely enhanced.
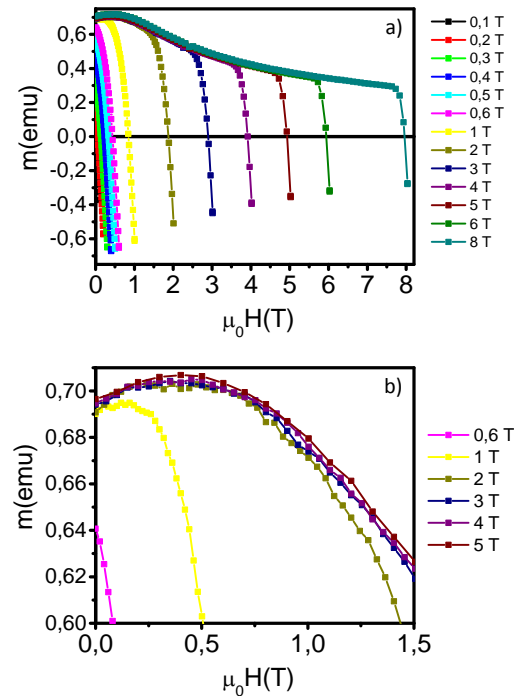

Figure 9. Hysteresis loops at different fields in a GdBCO-LF film grown with the Flash-Heating process showing a displacement of the maximum of the magnetization.

3.3 GdBCO-Gd$_2$O$_3$ nanocomposites. The preparation of GdBCO+20 mol % Gd$_2$O$_3$ nanocomposite films has been carried out following the solution methodology described in 2.1 and the flash heating process described in 2.1 and the flash heating process described in 3.2.

The XRD patterns of the nanocomposite films after the conversion process are shown in figure 10. They show epitaxial c-axis orientation of the GdBCO grains but the broadening of the (00l) spots suggests some degree of misorientation, figure 10 a). The peaks corresponding to Gd$_2$O$_3$ can be also observed, both in figures 10 b) and c). This confirms the formation of the Gd$_2$O$_3$ phase during the growth process. The presence of Gd$_2$O$_3$ nanoparticles (NPs) within the GdBCO matrix leads to an increased nanostrain reaching values of 0.24±0,01%, higher than pristine GdBCO-LF films (0.13±0,01%). Also the nanostrain obtained in these nanocomposites is comparable with the values obtained for CSD YBCO nanocomposites[38,66]. Nevertheless, it has to be taken into account that, very likely, this value of the strain has, in addition to a contribution from the

nanostrain arising from defects, some contribution associated to mesostrain (strain at grain boundaries) owing to the observation of some granularity effects [58].
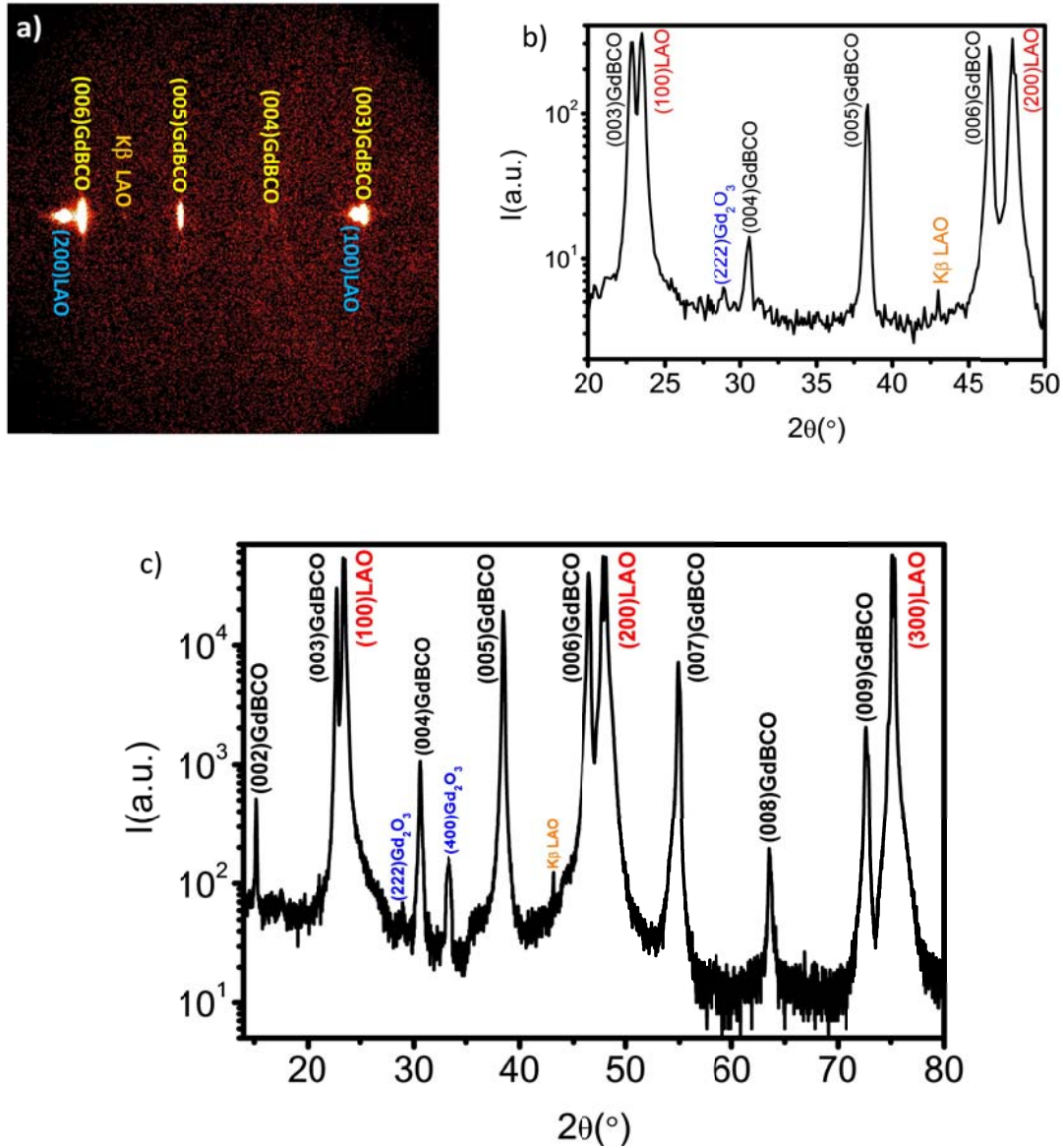

Figure 10. a) 2D XRD θ-2θ frame, b) integrated pattern from a) and c) high resolution pattern of a GdBCO-LF+20 mol % Gd$_2$O$_3$ film grown using the Flash-Heating process at 820 °C.

The TEM analysis shows perfectly c-axis oriented GdBCO grains, together with a random distribution of 30-50 nm Gd$_2$O$_3$ NPs (red arrows) in figure 11 a). Also, it is possible to distinguish the presence of Stacking Faults (SFs) in figures 11 b) – d) (white arrows) which have been recently shown to have a peculiar defect structure and display ferromagnetic properties[67]. Figure 11 d) shows the presence of superposed Gd$_2$O$_3$ NPs within the GdBCO matrix causing the formation of SFs at the interfaces.
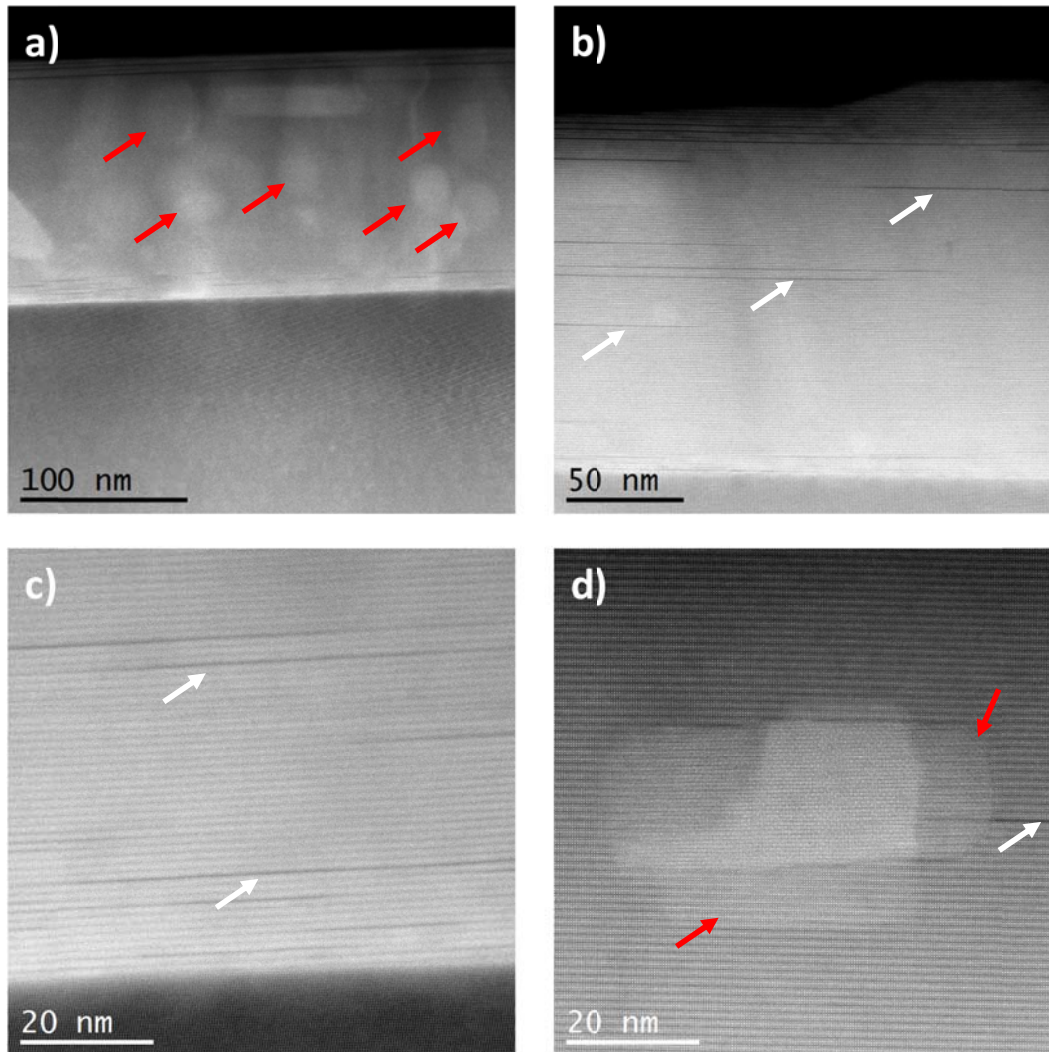
Figure 11. (a) LAADF and (b-d) HAADF STEM images of a GdBCO-LF+20 mol % Gd$_2$O$_3$ film grown with the flash-heating process at 820 °C a) A random distribution of 30-50 nm Gd$_2$O$_3$ NPs is observed with the matrix of the film causing the presence of SFs marked white arrows in b), c) and d). Picture d) shows two superimposed Gd$_2$O$_3$ NPs.

The superconducting properties of the GdBCO-LF+20 mol % Gd$_2$O$_3$ nanocomposites are improved with respect to the pristine GdBCO-LF films. The ρ(T) curve shown in figure 12 a) display a T_c (value of T at 50% of the transition) of ~ 91.7 K with a ΔT_c ~ 3.5 K ($\Delta T_c = T_{c,90}$- $T_{c,10}$). Figure 12 b) displays the $J_c(T)$ curve in which we can observe that the J_c^{sf} at 77 K reaches 3.2 MA/cm^2 while the J_c^{sf} at 5 K arrives at 24.7 MA/cm^2.
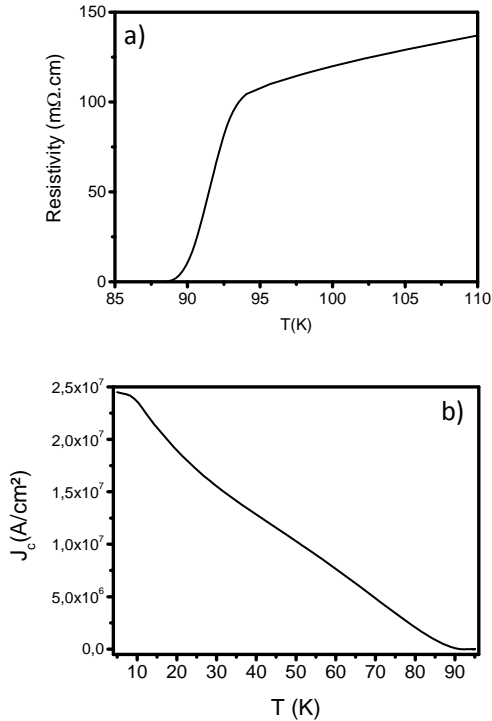
Figure 12. Superconducting properties of a GdBCO-LF+20 mol % Gd$_2$O$_3$ film grown with the flash-heating process at 820 °C extracted from a) the temperature dependence of the electrical resistivity ρ(T) and b) the temperature dependence of the inductively measured self-field J$_c$(T).

On the other hand, the strength of vortex pinning of the GdBCO-LF+20 mol % Gd$_2$O$_3$ nanocomposite films shown in the J_c / J_c^{sf} dependence at 77 K with the magnetic field (figure 13 a)) turned out to be enhanced, as compared to those of the reference pristine YBCO-TFA films, and similar to the reported values on GdBCO-TFA+BHO nanocomposite films[39]. The GdBCO+20 mol % Gd$_2$O$_3$ curve shows the typical smoothed field dependence that is commonly observed in the YBCO nanocomposites. Note that the curve for the GdBCO+20 mol % Gd$_2$O$_3$ film is very similar to the YBCO+10 mol % BZO nanocomposite films and much smoother than in the case of the pristine YBCO-TFA film. This demonstrates that the GdBCO+20 mol % Gd$_2$O$_3$ films have enhanced vortex pinning, at least at the same level as the YBCO+10 mol % BZO nanocomposites in films with similar thicknesses. The calculated B^* ($J_c(B^*)$=0.9J_c^{sf}) reach a value ~ 0.1 T which is in the range of the values reported for the

YBCO nanocomposites[41]. Finally, the analysis of the angular dependence of $J_c(\theta)$ and the isotropic collapse of the Irreversibility Line $H_{irr}(\theta)$ (figures 13 b) and 13 c)) has provided evidence of isotropic behavior in GdBCO-LF+20 mol % Gd$_2$O$_3$ nanocomposite films, similarly to the YBCO nanocomposites[38,40,41,66,68]. It is also remarkable the broadening of the peak at 90° (H//ab), associated to defects that are effective pinning centers close to the a-b plane and the vanishing of the peak at 0º (H||c), associated to a loss of effectiveness of correlated defects parallel to the c-axis. We attributed both peak evolutions to the presence of a large density of SFs, as we have seen in figure 11 that favor the accommodation of vortices at a broader angle range around the ab-planes and also cause strain-driven break of the c-oriented twin boundary coherence[69].

The anisotropic behaviour of the nanocomposite films can be characterized by a field-independent anisotropy parameter γ_{eff} when the anisotropic Ginzburg-Landau (AGL) scaling behaviour of $J_c(\theta,H)$ at fixed temperatures is studied. As proposed by Blatter et al.[70] and applied to REBCO films [68,71,72], the isotropic and anisotropic contributions to $J_c(\theta,H)$ and the Irreversibility Line $\mu_o H_{irr}(T)$ can be extracted from a plot of the effective field $H_{eff}=\varepsilon(\theta)H$, where $\varepsilon(\theta)=[\cos^2(\theta)+\gamma_{eff}^2\sin^2(\theta)]^{1/2}$ and γ_{eff} is the mass anisotropy ratio[37,38,68,72,73]. In our case, the GdBCO-LF+20 mol % Gd$_2$O$_3$ nanocomposite studied shows an effective γ_{eff} value of ~ 2.3 instead of the γ_{eff} ~ 5-7 value obtained for pristine YBCO-TFA films[37,38]. The γ_{eff} value found for our GdBCO-LF+20 mol % Gd$_2$O$_3$ nanocomposites is in the same range as YBCO nanocomposites suggesting that GdBCO nanocomposites display a similar vortex pinning landscape than YBCO nanocomposite films[38,40,41,66,68]. The origin of this reduction in γ_{eff} by the addition of nanoparticles has been associated to isotropic nanostrain and a novel depairing mechanism related to tensile strain fields in defects formed around the nanoparticles (especially in CSD-grown films)[37,38,74]. Other authors have also considered the contribution of geometrical effects for

sufficiently small[75], dirty-limit scattering and a change in coherence length anisotropy (discussed especially for PLD-grown films)[76].
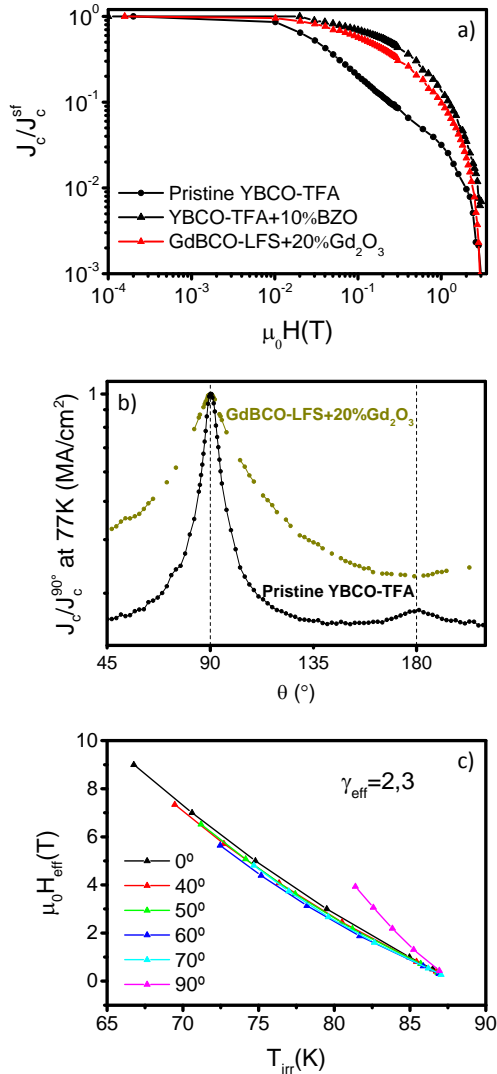
Figure 13. a) J_c/J_c^{sf} **dependence at 77 K with the magnetic field for the pristine YBCO-TFA and GdBCO-LF+20 mol % Gd$_2$O$_3$ films (it has been also included the dependences of the pristine YBCO and YBCO+10%M BZO films for comparison), b) angular dependence of the** $J_c/J_c^{90^o}$ **at 77 K and 1 T for the GdBCO-LF+20 mol % Gd$_2$O$_3$ films in comparison with a pristine YBCO-TFA film (films that are represented by the black curve with rounded symbols and the red curve in graph a)), and c) isotropic collapse of the Irreversibility Line** $\mu_oH_{irr}(T)$ **for the GdBCO-LF+20 mol % Gd$_2$O$_3$ nanocomposite, measured at different magnetic field orientations, with** γ_{eff} **~ 2.3.**

4. Conclusions

We have shown that the preparation of high critical current density GdBCO thin films by CSD is challenging requiring thorough optimization of the precursor solution formulation and designing a new high temperature thermal process. The sensitivity of the GdBCO-TFA solutions to the ambient humidity has led us to the development of a new Low-Fluorine solution to prepare GdBCO thin films by the CSD method. The developed GdBCO-LF solution solves the problem of reaching highly homogeneous films after the pyrolysis process. This novel solution avoids using high concentration of TFA salts (which are highly hygroscopic), and the presence of propionic acid while the use of TEA (coordination agents) help to prevent the water absorption that can derive in film buckling formation and degradation of the texture quality. Also, the presence of TEA gives to the system viscoelastic properties that help to release the stress generated due to the shrinkage during the pyrolysis without causing inhomogeneity. The use of this new solution allows to increase the rate of homogeneous films after the pyrolysis up to a 95% of success rate. The growth of epitaxial GdBCO-LF films required to design a new thermal profile, named "Flash-Heating" process with heating ramps ~600 ºC/min, to obtain full c-axis oriented GdBCO films. The superconducting properties of the resulting GdBCO-LF films are close to the best reported values so far. The T_c reaches 92.6 K while the J_c^{sf} at 77 K reaches ~1.5 MA/cm^2. However, this J_c value is still limited by granularity effects and, therefore, the Flash-Heating growth process should be still further optimized. The value of the J_c^{sf} at 77 K inside the grains has been estimated to be ~5 MA/cm^2 which suggests that there is still a lot of room for improvement. The Flash-Heating process was also shown to be a useful approach to grow epitaxial GdBCO+Gd$_2$O$_3$ nanocomposite films. These nanocomposite films show the typical features already observed for the CSD YBCO nanocomposite films (enhanced nanostrain and a large concentration of SFs) and also improved

superconducting properties as compared to pristine GdBCO-LF films reaching $T_{c,50} \sim$ 91.7 K and the J_c^{sf} at 77 K $\sim$3.2 MA/cm^2. The critical currents of the nanocomposites are, however, still limited by granularity effects and so further effort should be carried out to reach the highest performances.

Acknowledgements

References

1. X. Obradors and T. Puig, Coated conductors for power applications: materials challenges. *Supercond. Sci. Technol.* 27, 44003 (2014).

2. Y. Shiohara *et al.*, Future prospects of high T_c superconductors-coated conductors and their applications. *Phys. C Supercond.* 484, 1–5 (2013).

3. T. Izumi *et al.*, Development of TFA-MOD Process for Coated Conductors in Japan. *IEEE Trans. Appl. Supercond.* 19, 3119–3122 (2009).

4. T. Izumi *et al.*, Progress in development of advanced TFA-MOD process for coated conductors. *Phys. C Supercond. its Appl.* 463, 510–514 (2007).

5. K. Kimura *et al.*, Development of REBCO Coated Conductors by TFA-MOD Method With High Characteristic in Magnetic Field. *IEEE Trans. Appl. Supercond.* 23, 6601704–6601704 (2013).

6. H. C. Freyhardt *et al.*, Coated conductors and their applications. *Supercond. Sci. Technol.* 23, 010201–010201 (2010).

7. M. Murakami *et al.*, Melt-processed light rare earth element - Ba - Cu - O. *Supercond. Sci. Technol.* 9, 1015–1032 (1996).

8. B. J. Kim *et al.*, New MOD solution for the preparation of high J_c REBCO superconducting films. *Phys. C Supercond. its Appl.* 445, 582–586 (2006).

9. Y. Yoshida *et al.*, Progress in development of advanced PLD process for high J_c REBCO film. *Phys. C Supercond.* 468, 1606–1610 (2008).

10. C. Andreouli and A. Tsetsekou, Synthesis of HTSC Re(Y)Ba$_2$Cu$_3$O$_x$ powders: the role of ionic radius. *Phys. C Supercond.* 291, 274–286 (1997).

11. J. L. MacManus-Driscoll *et al.*, Systematic enhancement of in-field critical current density with rare-earth ion size variance in superconducting rare-earth barium cuprate films. *Appl. Phys. Lett.* 84, 5329–5331 (2004).

12. J. L. MacManus-Driscoll *et al.*, Rare earth ion size effects and enhanced critical current densities in Y$_{2/3}$Sm$_{1/3}$Ba$_2$Cu$_3$O$_{7-x}$ coated conductors. *Appl. Phys. Lett.* 86, 32505 (2005).

13. J. L. MacManus-Driscoll *et al.*, Studies of structural disorder in ReBa$_2$Cu$_3$O$_{7-x}$ thin films (Re=rare earth) as a function of rare-earth ionic radius and film deposition conditions. *Phys. C Supercond.* 232, 288–308 (1994).

14. M. S. Islam and R. C. Baetzold, Atomistic simulation of dopant substitution in YBa$_2$Cu$_3$O$_7$. *Phys. Rev. B* 40, 10926–10935 (1989).

15. J. L. Macmanus Driscoll, Materials chemistry and thermodynamics of REBa$_2$Cu$_3$O$_{7-x}$. *Adv. Mater.* 9, 457–473 (1997).

16. M. Erbe *et al.*, Improved REBa$_2$Cu$_3$O$_{7-x}$ (RE = Y, Gd) structure and superconducting properties by addition of acetylacetone in TFA-MOD precursor solutions. *J. Mater. Chem. A* 2, 4932 (2014).

17. L. H. Jin *et al.*, Fabrication of GdBa$_2$Cu$_3$O$_{7-x}$ films by TFA-MOD process. *J. Alloys Compd.* 509, 3353–3356 (2011).

18. J. H. Durrell *et al.*, A trapped field of 17.6 T in melt-processed, bulk Gd-Ba-Cu-O reinforced with shrink-fit steel. *Supercond. Sci. Technol.* 27, 82001 (2014).

19. T. Iguchi *et al.*, Fabrication of Gd Ba Cu O films by the metal organic deposition method using trifluoroacetates. *Supercond. Sci. Technol.* 15, 1415–1420 (2002).

20. A. Kaneko *et al.*, Fabrication of REBa$_2$Cu$_3$O$_{7-y}$ film by advanced TFA-MOD process. *Phys. C Supercond.* 412, 926–930 (2004).

21. Y. Iye *et al.*, Critical Field Anisotropy of a Single Crystal GdBa$_2$Cu$_3$O$_x$ and HoBa$_2$Cu$_3$O$_x$. *Jpn. J. Appl. Phys.* 26, L1850–L1852 (1987).

22. A. Gold *et al.*, The Magnetic Properties of the High-T_c Superconductor Gd-Ba-Cu-O: Bulk and Ring Structures. *Europhys. Lett.* 4, 1409–1414 (1987).

23. R. Krupke *et al.*, Superconducting, structural and surface properties of GdBaCuO thin films deposited by electron cyclotron resonance supported sputtering. *Phys. C Supercond.* 279, 153–164 (1997).

24. W. Andrä *et al.*, Rotational hysteresis losses in sputtered rebco films of different structure. *Phys. C Supercond.* 185–189, 2169–2170 (1991).

25. Q. Luo *et al.*, Effect of the O_2 /Ar Pressure Ratio on the Microstructure and Surface Morphology of Epi-MgO/IBAD-MgO Templates for $GdBa_2Cu_3O_{7-\delta}$ Coated Conductors. *Chinese Phys. Lett.* 31, 37402 (2014).

26. Y. Wang *et al.*, Dependencies of microstructure and stress on the thickness of $GdBa_2Cu_3O_{7-\delta}$ thin films fabricated by RF sputtering. *Nanoscale Res. Lett.* 8, 304 (2013).

27. S. Lee *et al.*, Development of In-Plume Pulsed Laser Deposition of High-I_c GdBCO Films for Coated Conductors. *IEEE Trans. Appl. Supercond.* 19, 3192–3195 (2009).

28. W. Li *et al.*, Fabrication of $GdBa_2Cu_3O_{7-\delta}$ films by photo-assisted-MOCVD process. *Phys. C Supercond.* 501, 1–6 (2014).

29. X. Obradors et al., Progress towards all-chemical superconducting $YBa_2Cu_3O_7$-coated conductors. *Supercond. Sci. Technol.* 19, S13–S26 (2006).

30. X. Obradors *et al.*, Chemical solution deposition: a path towards low cost coated conductors. *Supercond. Sci. Technol.* 17, 1055–1064 (2004).

31. X. Obradors *et al.*, Growth, nanostructure and vortex pinning in superconducting $YBa_2Cu_3O_7$ thin films based on trifluoroacetate solutions. *Supercond. Sci. Technol.* 25, 123001 (2012).

32. A. Gupta *et al.*, Superconducting oxide films with high transition temperature prepared from metal trifluoroacetate precursors. *Appl. Phys. Lett.* 52, 2077–2079 (1988).

33. J. W. Lee *et al.*, High-J_c $GdBa_2Cu_3O_{7-\delta}$ films fabricated by the metal–organic deposition process. *Phys. C Supercond. its Appl.* 470, 1253–1256 (2010).

34. G. Kim *et al.*, Optimal growth conditions for $GdBa_2Cu_3O_7$ thin-film coated conductors characterized by polarized Raman scattering spectroscopy. *Phys. C Supercond. its Appl.* 470, 1021–1024 (2010).

35. T. Iguchi *et al.*, Fabrication of GdBaCuO films by the metal organic deposition method using trifluoroacetates. *Supercond. Sci. Technol.* 15, 1415–1420 (2002).

36. Y. Sutoh *et al.*, Fabrication of high I_c film for GdBCO coated conductor by continuous in-plume PLD. *Phys. C Supercond.* 469, 1307–1310 (2009).

37. J. Gutiérrez *et al.*, Strong isotropic flux pinning in solution-derived $YBa_2Cu_3O_{7-x}$ nanocomposite superconductor films. *Nat. Mater.* 6, 367–373 (2007).

38. A. Llordés *et al.*, Nanoscale strain-induced pair suppression as a vortex-pinning mechanism in high-temperature superconductors. *Nat. Mater.* 11, 329–336 (2012).

39. M. Erbe *et al.*, $BaHfO_3$ artificial pinning centres in TFA-MOD-derived YBCO and GdBCO thin films. *Supercond. Sci. Technol.* 28, 114002 (2015).

40. P. Cayado *et al.*, Epitaxial $YBa_2Cu_3O_{7-x}$ nanocomposite thin films from colloidal solutions. *Supercond. Sci. Technol.* 28, (2015).

41. K. De Keukeleere *et al.*,Superconducting $YBa_2Cu_3O_{7-\delta}$ Nanocomposites Using Preformed ZrO_2 Nanocrystals: Growth Mechanisms and Vortex Pinning Properties. *Adv. Electron. Mater.* 1600161 (2016).

42. S. Engel *et al.*, Enhanced flux pinning in $YBa_2Cu_3O_7$ layers by the formation of nanosized $BaHfO_3$ precipitates using the chemical deposition method. *Appl. Phys. Lett.* 90, 102505 (2007).

43. X. Palmer *et al.*, Solution design for low-fluorine trifluoroacetate route to $YBa_2Cu_3O_7$ films. *Supercond. Sci. Technol.* 29, 24002 (2016).

44. Y. Chen *et al.*, High perfomance $GdBa_2Cu_3O_{7-x}$ Superconducting Film Prepared Using an Advanced Low-Fluorine Solution. *IEEE Trans. Appl. Supercond.* 22, 6601204–6601204 (2012).

45. W. Wu *et al.*, A low-fluorine solution with a 2:1 F/Ba mole ratio for the fabrication of YBCO films. *Supercond. Sci. Technol.* 27, 55006 (2014).

46. K. Zalamova *et al.*, Smooth Stress Relief of Trifluoroacetate Metal-Organic Solutions for $YBa_2Cu_3O_7$ Film Growth. *Chem. Mater.* 18, 5897–5906 (2006).

47. A. Llordés *et al.*, Evolution of Metal-Trifluoroacetate Precursors in the Thermal Decomposition toward High-Performance $YBa_2Cu_3O_7$ Superconducting Films. *Chem. Mater.* 22, 1686–1694 (2010).

48. P. C. McIntyre *et al.*, Effect of growth conditions on the properties and morphology of chemically derived epitaxial thin films of $Ba_2YCu_3O_{7-x}$ on (001) $LaAlO_3$. *J. Appl. Phys.* 71, 1868 (1992).

49. T. Araki *et al.*, Large-area uniform ultrahigh-J_c $YBa_2Cu_3O_{7-x}$ film fabricated by the metalorganic deposition method using trifluoroacetates. *Supercond. Sci. Technol.* 14, L21–L24 (2001).

50. J. Zhang *et al.*, Characterization and Molecular Structures of Yttrium Trifluoroacetate Complexes with O- and N-Donors: Complexation vs. Hydrolysis. *Eur. J. Inorg. Chem.* 2005, 3928–3935 (2005).

51. L. H. Jin *et al.*, Effect of relative humidity on morphology of YBCO films prepared by CSD method. *Phys. C Supercond.* 470, 1257–1260 (2010).

52. S. Morlens *et al.*, Thickness control of solution deposited YBCO superconducting films by use of organic polymeric additives. *J. Mater. Res.* 22, 2330–2338 (2007).

53. J. T. Dawley *et al.*, Rapid processing method for solution deposited $YBa_2Cu_3O_{7-\delta}$ thin films. *Phys. C Supercond.* 402, 143–151 (2004).

54. J. W. Lee *et al.*, Stability phase diagram of $GdBa_2Cu_3O_{7-\delta}$ in low oxygen pressures. *J.*

Alloys Compd. 602, 78–86 (2014).

55. F. Taïr *et al*., Melting temperature of $YBa_2Cu_3O_{7-x}$ and $GdBa_2Cu_3O_{7-x}$ at subatmospheric partial pressure. *J. Alloys Compd.* 692, 787–792 (2017).

56. N. Roma *et al*., Acid anhydrides: a simple route to highly pure organometallic solutions for superconducting films. *Supercond. Sci. Technol.* 19, 521–527 (2006).

57. C. F. Sánchez-Valdés *et al*., In situ study through electrical resistance of growth rate of trifluoroacetate-based solution-derived $YBa_2Cu_3O_7$ films. *Supercond. Sci. Technol.* 28, 24006 (2015).

58. X. Obradors *et al*., Nucleation and mesostrain influence on percolating critical currents of solution derived $YBa_2Cu_3O_7$ superconducting thin films. *Phys. C Supercond.* 482, 58–67 (2012).

59. A. Queraltó *et al*., Unveiling the Nucleation and Coarsening Mechanisms of Solution-Derived Self-Assembled Epitaxial $Ce_{0.9}Gd_{0.1}O_{2-y}$ Nanostructures. *Cryst. Growth Des.* 17, 504–516 (2017).

60. M. Coll *et al.,* Stress-induced spontaneous dewetting of heteroepitaxial $YBa_2Cu_3O_7$ thin films. *Phys. Rev. B* 73, 75420 (2006).

61. E. Bartolomé *et al*., Universal correlation between critical current density and normal-state resistivity in porous $YBa_2Cu_3O_{7-x}$ thin films. *Supercond. Sci. Technol.* 20, 895–899 (2007).

62. A. Pomar *et al*., Porosity induced magnetic granularity in epitaxial $YBa_2Cu_3O_7$ thin films. *Phys. Rev. B* 73, 214522 (2006).

63. A. Palau *et al*., Simultaneous inductive determination of grain and intergrain critical current densities of $YBa_2Cu_3O_{7-x}$ coated conductors. *Appl. Phys. Lett.* 84, 230 (2004).

64. A. Palau *et al*., C. Simultaneous determination of grain and grain-boundary critical currents in $YBa_2Cu_3O_7$-coated conductors by magnetic measurements. *Phys. Rev. B* 75, 54517 (2007).

65. J. E. Evetts and B. A. Glowacki, Relation of critical current irreversibility to trapped flux and microstructure in polycrystalline $YBa_2Cu_3O_7$. *Cryogenics.* 28, 641–649 (1988).

66. M. Coll *et al*., Size-controlled spontaneously segregated Ba_2YTaO_6 nanoparticles in $YBa_2Cu_3O_7$ nanocomposites obtained by chemical solution deposition. *Supercond. Sci. Technol.* 27, 44008 (2014).

67. J. Gazquez *et al*., Emerging Diluted Ferromagnetism in High-T_c Superconductors Driven by Point Defect Clusters. *Adv. Sci.* 3, 1500295 (2016).

68. J. Gutiérrez *et al*., Anisotropy and strength of vortex pinning centers in $YBa_2Cu_3O_{7-x}$ coated conductors. *Appl. Phys. Lett.* 90, 162514 (2007).

69. R. Guzman *et al*., Strain-driven broken twin boundary coherence in $YBa_2Cu_3O_{7-\delta}$ nanocomposite thin films. *Appl. Phys. Lett.* 102, 81906 (2013).

70. G. Blatter *et al*., From isotropic to anisotropic superconductors: A scaling approach. *Phys. Rev. Lett.* 68, 875–878 (1992).

71. X. Xu *et al*., Angular dependence of the critical current density for epitaxial $YBa_2Cu_3O_{7-\sigma}$ thin film. *Solid State Commun.* 92, 501–504 (1994).

72. L. Civale *et al*., Angular-dependent vortex pinning mechanisms in $YBa_2Cu_3O_7$ coated conductors and thin films. *Appl. Phys. Lett.* 84, 2121–2123 (2004).

73. L. Civale *et al*., Understanding High Critical Currents in $YBa_2Cu_3O_7$ Thin Films and Coated Conductors. *J. Low Temp. Phys.* 135, 87–98 (2004).

74. G. Deutscher, The role of Cu-O bond length fluctuations in the high temperature superconductivity mechanism. *J. Appl. Phys.* 111, 112603 (2012).

75. C. J. van der Beek *et al*., Anisotropy of strong pinning in multi-band superconductors. *Supercond. Sci. Technol.* 25, 84010 (2012).

76. M. Malmivirta, *et al*. Dirty limit scattering behind the decreased anisotropy of doped $YBa_2Cu_3O_{7-\delta}$ thin films. *J. Phys. Condens. Matter* 28, 175702 (2016).